Journal of Materials Chemistry A

Accepted Manuscript

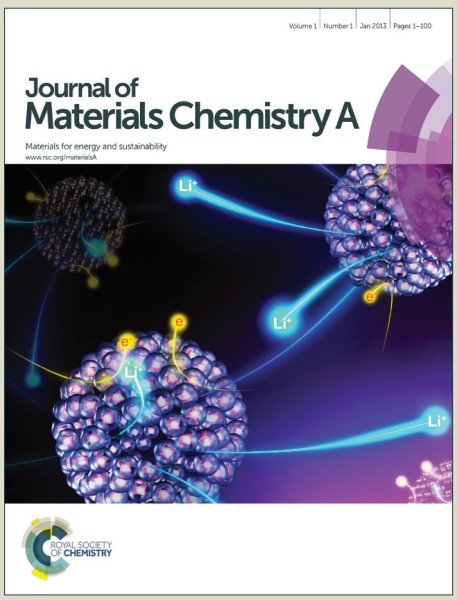

ROYAL SOCIETY OF CHEMISTRY

www.rsc.org/materialsA

Graphic Abstract

Amorphous 3D nanoflake array-assembled porous 2D cobalt-oxalate coordination polymer thin sheets with excellent pseudocapacitive performance

Lingyun Chen*[a,b], Qing Zhang[a], Xiaohuan Hou[a], Liying Xuan[a], Yuqian Jiang[a] and Yuan Yuan[a]

Abstract

Amorphous 3D nanoflake array-assembled porous 2D cobalt-oxalate coordination polymer thin sheets (CQU-Chen-OA-Co-1-1) were controlled synthesized and exhibited excellent pseudocapacitive performances.

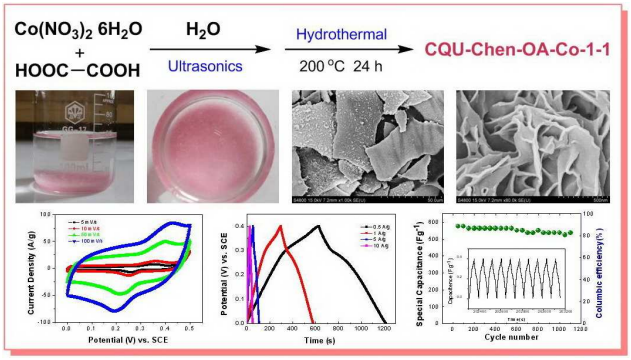

Cite this: DOI: 10.1039/c0xx00000x

www.rsc.org/xxxxxx

ARTICLE TYPE

Amorphous 3D nanoflake array-assembled porous 2D cobalt-oxalate coordination polymer thin sheets with excellent pseudocapacitive performance

Lingyun Chen*[a,b], Qing Zhang[a], Hong Xu[a], Xiaohuan Hou[a], Liying Xuan[a], Yuqian Jiang[a] and Yuan Yuan[a]

Received (in XXX, XXX) Xth XXXXXXXXX 20XX, Accepted Xth XXXXXXXXX 20XX
DOI: 10.1039/b000000x

Amorphous three-dimensional (3D) nanoflake array-assembled porous 2D cobalt-oxalate coordination polymer thin sheets (CQU-Chen-OA-Co-1-1) were first synthesized by using a facile hydrothermal route under electro-magnetic stirring. The resulting material exhibited excellent pseudocapacitive performance with high specific capacitance of 702.75 $F \cdot g^{-1}$ at 1 $A \cdot g^{-1}$ and remarkable cycling stability.

With the increasing demand of clean and renewable energy, more urgent efforts have been devoted to the development of efficient and reliable energy storage and conversion devices.[1] Supercapacitors (SCs), also known as electrochemical capacitors (ECs), can repeatedly generate clean electricity from stored materials and convert electric energy into chemical energy reversibly. Because of their excellent properties such as high power density, fast recharge capability, high specific capacitance, long cycle life and excellent cycling stability, SCs are regarded as a promising energy storage and conversion technology.[2] Depending on different charge storage mechanism, SCs can be categorized into electrochemical double layer SCs (EDLCs) and pseudocapacitors (PCs). The former utilize the capacitance arising from charge separation at an electrode/electrolyte interface, and the latter is mainly produced by fast faradaic reactions associated with double injection/extraction of ions and electrons. In general, PCs can offer higher capacitance values than EDLCs due to their fast and reversible redox reaction.[3] Therefore, much research attention has been focused on the development of pseudocapacitive materials for SCs.

Because of their unique structures, excellent properties and potential applications in various areas, complex nano-architectures constructed from the self-assembly of nano-building blocks with specific dimensions have attracted extensive interest.[4] And controlling of nano-building blocks into two- and three-dimensional (2D/3D) architectures will combine the features of micro- and nanostructures. Moreover, the energy storage ability of the SCs is determined by the choice and structure of the electrode materials. Furthermore, 2D/3D nano-architectures facilitate ion transport by providing smaller resistance and shorter diffusion pathways for SCs.[5] In

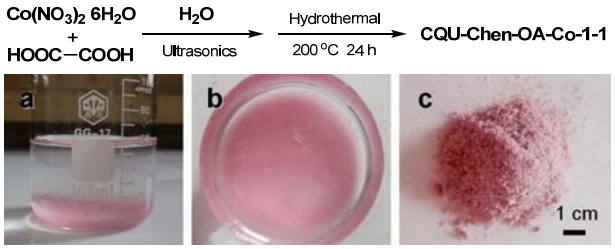

Fig. 1 Schematic illustration of the hydrothermal synthesis of the CQU-Chen-OA-Co-1-1 and corresponding digital photography of the samples (a) and (b) in 100 ml beaker after hydrothermal reaction and (c) after freeze-drying.

order to obtain SCs with high performance, recent studies have been focused on the fabrication of SCs electrode materials with complex architectures including metal oxide,[6] metal hydroxide and layered hydroxide,[7] metal chalcogenide,[8] carbon materials,[9] and conducting polymer,[10] as well as their corrresponding composites.[11] In particular, amorphous materials with nano-architectures including metal oxide (such as MnO_2, CuO and $NiWO_4$)[12] and metal hydroxide (such as $Ni(OH)_2$ and $Co(OH)_2$)[13] have shown superior electrochemical performance and been investigated for PCs recently due to their high theoretical capacitance, environment benignity and good pseudo-capacitive performance.[12,13] However, controlled synthesis of amorphous 2D/3D nano-architectures for high performance PCs via simple and facile methods still remains a significant challenge.

Meanwhile, recent years have witness the rapid development of coordination polymers (CPs) or metal–organic frameworks (MOFs) due to their intriguing structures, large surface areas and porosities as wel as various potential applications.[14] Different types of molecular building blocks, namely, the organic ligand, the metal ion (and the counterion) and the solvent (or mixture of solvents), are involved in the generation of CPs. And distinct self-assembly of these components will result in the formation of various inorganic–organic hybrid solids. Among them, the self-assembly of metal ion and oxalate dianion ($C_2O_4^{2-}$, ox) under hydrothermal or solvothermal conditions provides a rich variety of extended coordination networks for the design and synthesis of various 1D, 2D, and 3D CPs.[15] Up to date, one fascinating and

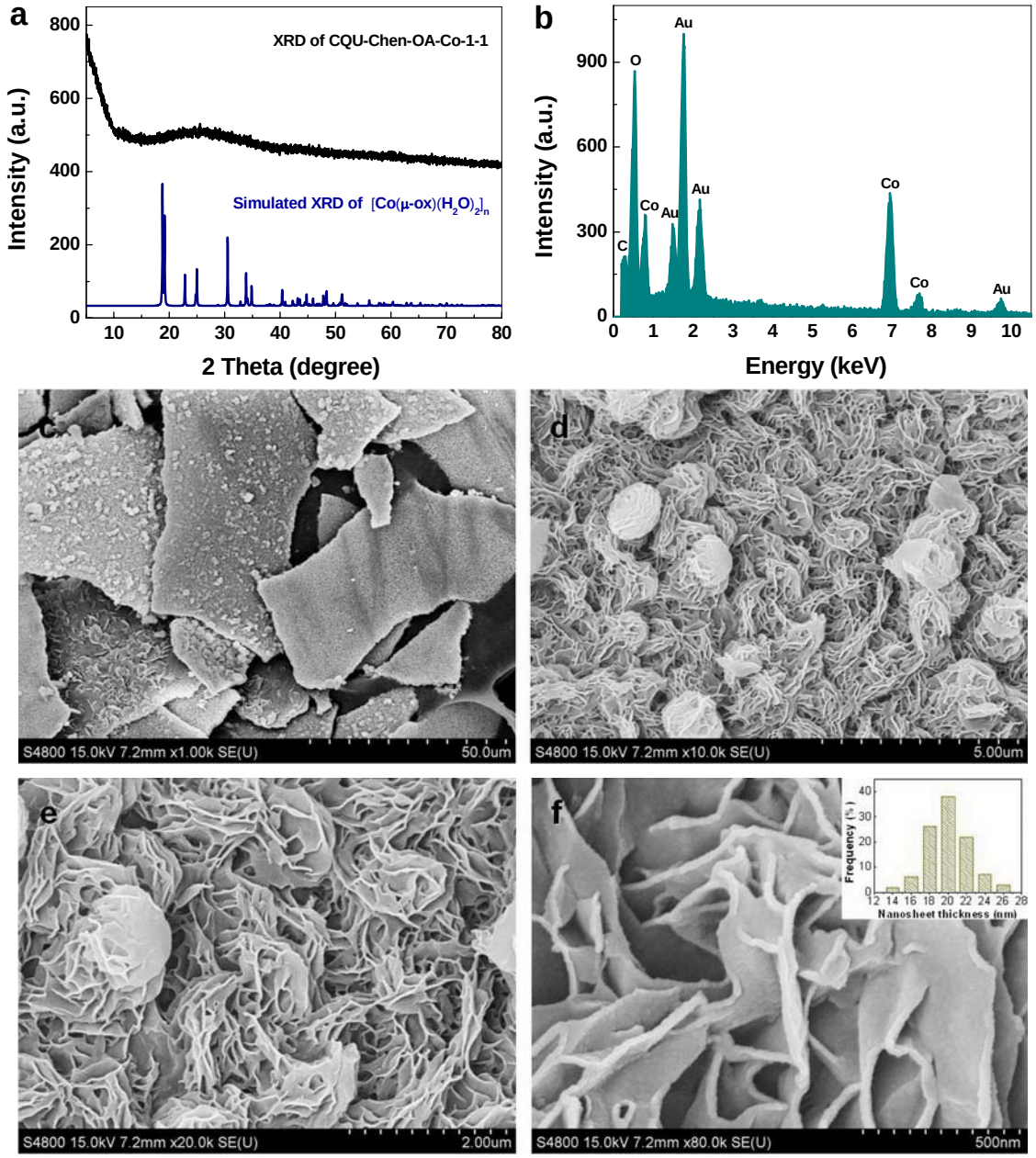

Fig. 2 (a) XRD patterns of the CQU-Chen-OA-Co-1-1 and simulated XRD patterns of $[Co(\mu\text{-}ox)(H_2O)_2]_n$, (b) EDX spectra, and (c)-(f) FE-SEM images at various magnification of the CQU-Chen-OA-Co-1-1. The inset of panel f presents the distribution of nanosheet thickness.

challenging synthetic target is self-assembly of 2D/3D CPs nano-architectures from molecular building blocks. Such a coordination-driven self-assembly will provide a facile means to achieve ordered and well-defined 2D/3D architectures from functional building blocks (molecular and nano-building blocks) with intriguing strtuctures and a variety of potential applications in gas storage and separation, catalysis, and energy storage especailly SCs.[4b,14c,16] In general, some CPs or MOFs crystals were used as precursors or templates for the fabrication of porous metal oxide[17], porous carbon materials[18] and their corresponding composites[19] as electrode materials for SCs. However, studies into the direct use of CPs or MOFs crystals as electrode materials for SCs are rarer because of their poor electrical conductivity, steric hindrance to ion insertion due to the pore size and incompatibility between the CPs crystals and the electrolyte.[20] To overcome above problems, it is necessary to controll the CPs crystal structures especailly 2D or 3D porous structures and structural architecture of the CPs is the key factor that control the reacting surface area and diffusion of active ions from electrolyte into the entire part of the CPs.[21] On the one hand, the porous CPs can solve the problem of insulating character by tuning of the linker structure which will result in the better charge transfer within the coordination frameworks of the CPs, while the redox behavior of metal cations could provide transport pathways for electrons.[22] On the other, the porous CPs may eliminate steric limitations by the electrolyte ion with its solvation shell and fully take advantage of the

micropores or other channels to permit quick electrolyte diffusion.[23] In addition, active metal cations in the porous CPs should be accompanied by matched electrolyte solution in order to ensure the predominant charge storage mechanism can manifest through a pseudocapacitive reaction and therefore exhibit high capacitance.[20b,24] Although simple oxalates such as NiC_2O_4 and MnC_2O_4 have been reported for electrode materials of SCs, [25] there is no report on the controlled self-assembly of amorphous metal-oxalic acid (OA) CPs nano-architectures with pseudocapacitive performance.

In the present work, we first report a simple and facile hydrothermal method for large-scale self-assembly of amorphous porous 2D cobalt-oxalate coordination polymer thin sheets (CQU-OA-Co-1-1) with interconnected channels and hierarchical porosity. The as-prepared products exhibit transparent pink sheet-like structures on a large scale especially in solution with digital photography in Fig. 1a and b. In this simple self-assembly process (see Fig. 1), OA was used as the ligand, cobalt (II) nitrate hexahydrate ($Co(NO_3)_2{\cdot}6H_2O$) as the source of cobalt source, and Water as the solvent (see experimental detail in ESI†). All the regents were purchased from Sinopharm Chemical Reagent Co. and used as received without further purification. In a typical procedure, 0.001 mol $Co(NO_3)_2{\cdot}6H_2O$ and 0.001 mol OA were added into 40 mL distilled water, followed by ultrasonics for 30 min. The resulting solution was transferred into a 50 mL of Teflon-lined autoclave, which was maintained at 200 °C for 24 h under electro-magnetic stirring for 500 rpm and then cooled to room temperature naturally. A pink colour product was collected by centrifuging and washed with water and absolute ethanol several times. Subsequently, these precipitates were frozen for 2 h followed by freeze-drying overnight. Impressively, the as-obtained CQU-Chen-OA-Co-1-1 exhibited high specific capacitance and remarkable cycling stability as an electrode material for SCs.

The crystallographic structure and phase purity of the CQU-Chen-OA-Co-1-1 are evaluated by X-ray powder diffraction (XRD) as shown in Fig. 2a. The sample appears its amorphous feature, as indicated by a broad peak located at a 2θ value of around 25° and the lack of other diffraction peaks from crystallinephases.[26] In addition, the compositions of the CQU-Chen-OA-Co-1-1 were investigated through the energy dispersive X-ray analysis (EDX) inset in Fig. 2b and results demonstrates that the sample is composed of the elements of Co, C, O, and Au, and Au came from the prinkled Au for SEM examination of the sample. Based on above analysis and along with Fourier transformsinfrared spectra (FT-IR) in Fig. S3 and thermogravimetric-differential thermal analysis (TGA-DTA) in Fig. S4 with detailed analysis in ESI, the CQU-Chen-OA-Co-1-1 dispalys CPs structure with the composition and structure of $[Co(\mu\text{-ox})(H_2O)_2]_n$ in Fig. S5.

The size and morphology of the CQU-Chen-OA-Co-1-1 were observed by scanning electron microscopy (SEM) in Fig. 2c-f. From the low magnification SEM image in Fig. 2c, large-scale of 2D sheets with a lateral size altering from tens to hundreds of micrometers and a thickness of about 20 μm were obtaind. Further investigation on the high magnification SEM images (in Fig. 2d-f) declares that the sample is composed of numerous ultrathin nanoflakes in very high density which are interconnected with each other to form a 3D open network-like microstructure. The surface of the nanoflakes is smooth with thicknesses of ca. 20 ± 3 nm (inset in Fig. 4d). In addition, the N_2 adsorption and desorption isotherms and pore-size distribution plot of the CQU-Chen-OA-Co-1-1 in Fig. S6 reveals a mesoporous structure as a type-IV adsorption branch according to IUPAC classification with specific surface area of 67.25 $m^2\ g^{-1}$, and pore volume of 150 $m^3{\cdot}g^{-1}$ with average pore sizes at 3.6 nm and >10 nm, which is possible attributed to the multi-peak distribution including both mesopores and macropores by the assemly of the nanosheets and is in agreement with results from SEM studies (in Fig. 2c-f).

The electrochemical properties of the CQU-Chen-OA-Co-1-1 as electrode materials for SCs were evaluated by cyclic voltammetry (CV), galvanostatic charge−discharge (GCD) measurement and electrochemical impedance spectroscopy (EIS) in 2.0 M KOH solution. The CV curves of the CQU-Chen-OA-Co-1-1 in the voltage window of 0-0.5 V at different scan rates from 5 to100 mV s^{-1} is in Fig. 3a. The CV profile show oxidation (anodic) and reduction (cathodic) events, which are PCs. Redox peaks are observed at all scan rates, which corresponds to the conversion between different oxidation/reduction states of cobalt. With the increase of scan rate, the current response increases accordingly, and the peak shapes are well retained even at a high scan rate of 100 $mV{\cdot}s^{-1}$, indicating a good rate capability. Moreover, the asymmetric and scan rate dependent shape of the CV profiles reveal that the origin of the capacitance is derived from the faradic reaction and good reversibility of the oxidation and reduction processes. In addition, the anodic peaks become more positive and the cathodic peaks become more negative with the increased scan rate because of an increasing polarization at high scan rate. And the contribution of pure Ni foam to the capacitance of the CQU-Chen-OA-Co-1-1 electrode is small and can be ignored.

The GCD curves of the CQU-Chen-OA-Co-1-1 electrode at different current densities in the potential window of 0–0.5 V is shown in Fig. 3b. From which, the corresponding specific capacitances were 731.25, 702.75, 690, 675.75, 666, 656.25 and 612.5 $F{\cdot}g^{-1}$ at current densities of 0.5, 1, 2, 3, 4, 5, and 10 $A{\cdot}g^{-1}$, respectively, as plotted in Fig. 3c. And 83.76 % of the initial capacitance could be retained when the current density increased from 0.5 to 10 $A{\cdot}g^{-1}$, indicating the excellent rate capability of the as-prepared electrode. With increasing scan rate, the specific capacitance decreases gradually, which can be attributed to electrolytic ions diffusing and migrating into the active materials at low scan rates. At high scan rates, the diffusion effect, limiting the migration of the electrolytic ions, causes some active surface areas to become inaccessible for charge storage. This result indicates the excellent capacitive behavior and high-rate capability of the amorphous phase. On the basis of the galvanostatic charge–discharge curves at different current densities in Fig. 3b, the energy and power densities of CQU-Chen-OA-Co-1-1 were calculated. From the Ragone plot in Fig. 3d, high energy density is observed for the CQU-Chen-OA-Co-1-1 electrode in 2 M KOH.

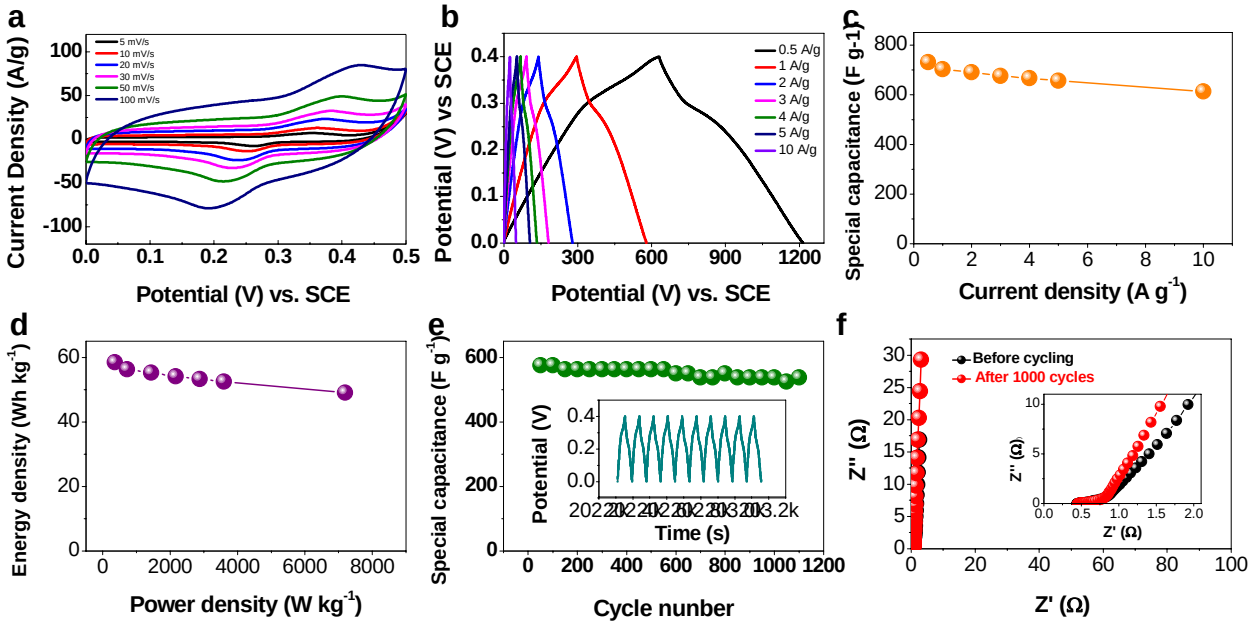

Fig. 3 Electrochemical performance of the CQU-Chen-OA-Co-1-1-based electrodes: a) CV curves at different scan rates; b) charge–discharge profiles at various current densities; c) correlation profiles of the scan rate and specific capacitance; d) plots of power density versus energy density; e) The GCD cycling-performance and the Coulombic-efficiency profiles at 5 $A \cdot g^{-1}$; and f) EIS plots before cycling and after 1000 cycles at open circuit potential, the insert is the portion of magnification pattern.

The cycling stability of the CQU-Chen-OA-Co-1-1 electrode is evaluated by GCD measurement over 1000 cycles at a constant current densities of 5$A \cdot g^{-1}$ (in Fig. 3e). The specific capacitance of the as-prepared electrode increases gradually up to 656.25 $F \cdot g^{-1}$ in the course of the initial 1000 cycles, which can be attributed to the full activation of the present electrode. After extended cycling to 1000 cycles, 94.3 % of the capacitance at the 1000 cycle can still be maintained, evidently showing its superior cycling stability.

In addition, the EIS measurements were carried out to determine the electrode kinetics within the frequency range from 0.01 Hz to 100 kHz under AC voltage amplitude of 5 mV. The Nyquist plots of the CQU-Chen-OA-Co-1-1 electrode before and after 1000 cycles are illustrated in Fig. 3f. From which, each Nyquist plot basically has a depressed small semicircle in the high-frequency region and a straight line in the low-frequency region. The semicircle in the high frequency range is attributed to the three sections: electrolyte, electroactive material and the contact resistance between the electroactive material and the current collector, and the straight line is related to the diffusive resistance. At very high frequencies, the intercept at the real axis (Z′) represents equivalent series resistance (ESR) including the inherent resistance of the electroactive material, the bulk resistance of electrolyte, and the contact resistance at the active material/current collector interface.[6,7,27] The ESR value was found to be 0.44 and 0.46 Ω before and after 1000 cycles, respectively. This low ESR value indicates that the CQU-Chen-OA-Co-1-1 is highly conductive and that there is excellent electrical contact between the CQU-Chen-OA-Co-1-1 nanosheet arrays and Ni foam substrate. This is characteristic of capacitive behavior, and representative of the ion diffusion in the electrode structure, indicating that the electrode behaves more closely as an ideal capacitor. Moreover, the semicircle is associated with electrode surface properties and corresponds to the Faradic charge-transfer resistance (Rct), which is well-known to limit rate capability in SCs. In addition, the diameter of the semicircle for the CQU-Chen-OA-Co-1-1 nanosheet array electrode is small in Fig. 3f, which reveals a low Rct. There is no obvious difference between the 1st and 1000th cycles, indicating that the CQU-Chen-OA-Co-1-1 is suitable for SCs.

All results from the electrochemical measurements indicate that the CQU-Chen-OA-Co-1-1 is one kind of promising electrode materials for PCs. The high energy storage ability of the CQU-Chen-OA-Co-1-1 was attributed to the following structural features. Firstly, the hierarchical porosity of the CQU-Chen-OA-Co-1-1 largely increases the amount of electroactive sites. In addition, the interconnected channels formed by the interconnected nanosheet-building blocks greatly facilitates transport of the electrolyte. As a result, the CQU-Chen-OA-Co-1-1 offer an efficient charge-transfer pathway with significantly lower contact resistance, thus highlighting their potential as advanced energy-storage electrode materials.

In summary, we have reported the controlled synthesis of amorphous porous 2D cobalt-oxalate coordination polymer thin sheets (CQU-Chen-OA-Co-1-1) with 3D nanoflake array sttructures using a facile hydrothermal method. The amorphous CQU-Chen-OA-Co-1-1 with interconnected channels and hierarchical porosity exhibit oustanding electrochemical behaviors for PCs. We believe that such a route will undoubtedly become an essential synthetic strategy in the design and synthesis of novel functional CPs or MOFs nanostructures and bring more opportunities to the research and real applications of CPs or MOFs, as well as rapid

development of new electrode materials with high performance for SCs.

This work is supported by the National Natural Science Foundation of China (No. 21101176), the Natural Science Foundation Project of CQ CSTC (No. 2010BB4232), the Fundamental Research Funds for the Central Universities (No. CQDXWL-2012-014 and CQDXWL-2012-037), and the Open Foundation of the State Key Laboratory of Coordination Chemistry of Nanjing University.

Notes and references

[a] *Department of Applied Chemistry, School of Chemistry and Chemical Engineering, Chongqing University, Chongqing 400044, China. E-mail: lychen@cqu.edu.cn*

[b] *State Key Laboratory of Coordination Chemistry, Nanjing University, Nanjing 210093, China*

† Electronic Supplementary Information (ESI) available: details of experimental and characterization as well as additional figures. See DOI: 10.1039/b000000x/

‡ Footnotes should appear here. These might include comments relevant to but not central to the matter under discussion, limited experimental and spectral data, and crystallographic data.

1 (a) B. Dunn, H. Kamath and J. M. Tarascon, *Science*, 2011, **334**, 928-935, (b) X. F. Wang, X. H. Lu, B. Liu, D. Chen, Y. X. Tong and G. Z. Shen, *Adv. Mater.* 2014, **26**, 4763-4782.

2 (a) P. Simon, Y. Gogotsi and B. Dunn, *Science*, 2014, **343**, 1210-1211; (b) Y. Gogotsi, and P. Simon, *Science*, 2011, **334**, 917-918; (c) C. Z Yuan, H. B. Wu, Y. Xie and X. W. Lou, *Angew. Chem. Int. Ed.*, 2014, **53**, 1488-1504; (d) V. Augustyn, P. Simon and B. Dunn, *Energy Environ. Sci.*, 2014, **7**, 1597-1614.

3 B. E. Conway, Electrochemical Supercapacitor Scientific Fundamentals and Technological Applications, Springer, 1999.

4 (a) L. Zhang, H. B. Wu, S. Madhavi, H. H. Hng and X. W. Lou, J. *Am. Chem. Soc.*, 2012, **134**, 17388–17391; (b) Z. Zhang, Y. Chen, S. He, J. Zhang, X. Xu, Y. Yang, F. Nosheen, F. Saleem, W. He and X. Wang, *Angew. Chem. Int. Ed.*, 2014, DOI: 10.1002/anie.201406484.

5 (a) P. Simon and Y. Gogotsi, *Nat. Mater.*, 2008, **7**, 845-854; (b) Q. F. Zhang, E. Uchaker, S. L. Candelariaza and G. Z. Cao, *Chem. Soc. Rev.*, 2013, **42**, 3127-3171; (c) K. K. Lee, W. S. Chin and C. H. Sow, *J. Mater. Chem. A*, 2014, DOI: 10.1039/C4TA02074J; (d) L. Feng, Y. Zhu, H. Ding and C. Ni, *J. Power Sources*, 2014, **267**, 430-444.

6 (a) J. Jiang, Y. Y. Li, J. P. Liu, X. T. Huang, C. Z. Yuan and X. W. Lou, *Adv. Mater.* 2012, **24**, 5166-5180; (b) H. B. Wu, H. Pang and X. W. Lou, *Energy Environ. Sci.*, 2013, **6**, 3619-3626; (c) Q. Wang, X. Wang, B. Liu, G. Yu, X. Hou, D. Chen and G. Z. Shen, *J. Mater. Chem. A*, **2013**, 1, 2468-2473; (d) H. N. Zhang, Y. J. Chen, W. W. Wang, G. H. Zhang, M. Zhuo, H. M. Zhang, T. Yang, Q. H. Li and T. H. Wang, *J. Mater. Chem. A*, 2013, 1, 8593-8600; (e) L. F. Shen, Q. Che, H. S. Li and X. G. Zhang, *Adv. Funct. Mater.*, 2014, **24**, 2630-2637..

7 (a) L. Huang, D. C. Chen, Y. Ding, S. Feng, Z. L. Wang and M. L. Liu, *Nano Lett.*, 2013, **13**, 3135-3139; (b) H. Chen, L. Hu, Min Chen, Y. Yan and L. M. Wu, *Adv. Funct. Mater.*, 2014, **24**, 934-942; (c) J. W. Zhao, J. Chen, S. M. Xu, M. F. Shao, Q. Zhang, F. Wei, J. Ma, M. Wei, D. G. Evans and X. Duan, *Adv. Fuct. Mater.*, 2014, **24**, 2938-2946; (d) J. Pu, Y. Tong, S. Wang, E. Sheng and Z. H. Wang, *J. Power Sources*, 2014, **250**, 250-256.

8 (a) X. Wang, B. Liu, Q. Wang, W. Song, X. Hou, D. Chen, Y. Cheng and G. Z. Shen, *Adv. Mater.*, 2013, **25**, 1479-1486; (b) L. Mei, T. Yang, C. Xu, M. Zhang, L. B. Chen, Q. H. Li and T. H. Wang, *Nano Energy*, 2014, **3**, 36-45; (c) X. H. Rui, H. T. Tan and Q. Y. Yan, *Nanoscale*, 2014, **6**, 9889-9924; (d) H. H. Huo, Y. P. Zhao and C. L. Xu, *J. Mater. Chem. A*, 2014, **2**, 15111-15117.

9 (a) H. Jiang, P. S. Lee and C. Z. Li, *Energy Environ. Sci.*, 2013, **6**, 41-53; (b) W. Xia, B. Qiu, D. G. Xia and R. Q. Zou, *Scientific Reports*, 2013, **3**, 1935-1942; (c) J. Y. Liang, S. L. Chen, M. J . Xie, Y. Z. Wang, X. K. Guo, X. F. Guo and W. P. Ding, *J. Mater. Chem. A*, 2014, **2**, 16884-16891.

10 (a) K. Wang, H. Wu1, Y. Meng and Z. X Wei1, *Small*, 2014, **10**, 14-31; (b) G. A. Snook, P. Kao and A. S. Best, *J. Power Sources*, 2011, **196**, 1-12.

11 (a) Y. Hou, Y.Cheng , T. Hobson and J. Liu, *Nano Lett.*, 2010, **10**, 2727-2733; (b) Z. Chen, Y. Qin, D. Weng, Q. Xiao, Y. Peng, X. Wang, H. Li, F. Wei and Y. F. Lu, *Adv. Funct. Mater.*, 2009, **19**, 3420-3426; (c) J. Yan, T. Wei, Z. J. Fan, W. Qian, M Zhang, X Shen and F. Wei, *J. Power Sources*, 2010, **195**, 3041-3045.

12 (a) P. Yang, Y. Li, Z. Lin, Y. Ding, S. Yue, C. P. Wong, X. Cai, S. Tan and W. J. Mai, *J. Mater. Chem. A*, 2014, **2**, 595-599; (b) C. C. Hua, C. Y. Hunga, K. H. Chang and Y. L. Yang, J. Power Source, 2011, 196, 847-850; (c) B. Liu, X. Zhao, Y. Xiao and M. H. Cao, *J. Mater. Chem. A*, 2014, **2**, 3338-3343; (d) L. Niu, Z. Li, Y. Xu, J. Sun, W. Hong, X. Liu, J. Q. Wang and S. Rang, *ACS Appl. Mater. Interfaces*, 2013, **5**, 8044-8052; (e) Y. B. He, G. R. Li, Z. L. Wang, C. Y. Su and Y. X. Tong, *Energy Environ. Sci.*, 2011, **4**, 1288-1292.

13 (a) H. B. Li, M. H. Yu, F. X. Wang, P. Liu, Y. Liang, J. Xiao, C. X. Wang, Y. X. Tong and G. W. Yang, *Nat. Commun.*, 2013, **4**, 1894-1901; (b) H. B. Li, M. H. Yu, X. H. Lu, P. Liu, Y. Liang, J. Xiao, Y. X. Tong and G. W. Yang, *ACS Appl. Mater. Interfaces*, 2014, **6**, 745-749; (c) Y. Fu, J. M. Song, Y. Q. Zhu and C. B. Cao, *J. Power Sources*, 2014, **262**, 344-348.

14 (a) H. Furukawa, K. E. Cordova, M. O'Keeffe and O. M. Yaghi, *Science*, 2013, **341**, 974; (b) S. Kitagawa, R. Kitaura and S. Noro, *Angew. Chem. Int. Ed.*, 2004, **43**, 2334-2375; (c) J. M. Falkowski, T. Sawano, T. Zhang, G. Tsun, Y. Chen, J. V. Lockard and W. B. Lin, *J. Am. Chem. Soc.*, 2014, **136**, 5213-5216; (d) C. V.McGuire, R. S. Forgan, *Chem. Commun.*, 2014, DOI: 10.1039/C4CC04458D; (e) D. Y. Lee, D. V. Shinde, E. Kim, W. Lee, I. Oh, N. K. Shrestha, J. K. Lee and S. H. Han, *Microporous Mesoporous Mater.*, 2013, **171**, 53-57; (f) R. Díaz, M. G. Orcajo, J. A. Botas, G. Calleja and J. Palm, *Mater. Lett.*, 2012, **68**, 126-128; (g) G. de Combarieu, M. Morcrette, F. Millange, N. Guillou, J. Cabana, C. P. Grey, I. Margiolaki, G. Férey and J. M. Tarascon, *Chem. Mater.*, 2009, **21**, 1602-1611.

15 (a) C. N. R. Rao, S. Natarajan and R. Vaidhyanathan, *Angew. Chem. Int. Ed.,* 2004, **43**, 1466-1496; (b) M. B. Hursthouse, M. E. Light and D. J. Price, *Angew. Chem. Int. Ed.,* 2004, **43**, 472-475; (c) E. Cariati, R. Macchi, D. Roberto, R. Ugo, S. Galli, N. Casati, P. Macchi, A. Sironi, L. Bogani, A. Caneschi and D. Gatteschi, *J. Am. Chem. Soc.*, 2007, **129**, 9410-9420; (d) D. Armentano, G. De Munno, T. F. Mastropietro, M. Julve and F. Lloretb, *Chem. Commun.*, 2004, 1160-1161; (e) T. D. Keene, M. B. Hursthouse and D. J. Price, *Crys. Growth Des.*, 2009, **9**, 2604-2609.

16 (a) S. Furukaw, J. Reboul, S. Diring, K. Sumida and S Kitagawa, *Chem. Soc. Rev.*, 2014, **43**, 5700-5734; (b) Y. Yue, Z. Qiao, P. F. Fulvio, A. J. Binder, C. Tian, J. Chen, K. M. Nelson, X. Zhu and S. Dai, *J. Am. Chem. Soc.*, 2013, **135**, 9572-9575; (c) E. Breynaert, J, Emmerich, D. Mustafa , S. R. Bajpe, T. Altantzis, K. V. Havenbergh, F. Taulelle, S. Bals, G. V. Tendeloo, C. E. A. Kirschhock and J. A. Martens, *Adv. Mater.*, 2014, **26**, 5173-5178; (d) A. Carné-Sánchez, I. Imaz, M. Cano-Sarabia and D. Maspoch, *Nat. Chem.*, 2013, **5**, 203-211; (e) J. Guo, Y. Ping, H. Ejima, K. Alt, M. Meissner, J. J. Richardson, Y. Yan, K. Peter, D. von Elverfeldt, C. E. Hagemeyer and F. Caruso, *Angew. Chem. Int. Ed.*, 2014, **53**, 5546-5551; (f) W. B. Lin, W. J. Rieter and K. M. L. Taylor, *Angew. Chem. Int. Ed.*, 2009, **48**, 650-658.

17 F. Meng, Z. G. Fang, Z. X. Li, W. W. Xu, M. J. Wang, Y. P. Liu, J. Zhang, W. R. Wang, D. Y. Zhao and X. H. Guo, *J. Mater. Chem. A*, 2013, **1**, 7235-7241.

18 (a) A. J. Amali, J. K. Sun and Q. Xu, *Chem. Commun.*, 2014, **50**, 1519-1522; (b) P. Zhang, F. Sun, Z. G. Shen and D. P. Cao, *J. Mater. Chem. A*, 2014, **2**, 12873-12880.

19 K. B. Wang, X. Y. Ma, Z. Y. Zhang, M. B. Zheng, Z. R. Geng and Z. L. Wang, *Chem. Eur. J.*, 2013, **19**, 7084-7089.

20 (a) G. Combarieu, M. Morcrette, F. Millange, N. Guillou, J. Cabana, C. Grey, I. Margiolaki, G. Ferey and J. M. Tarascon, *Chem. Mater.*, 2009, **21**, 1602-1611; (b) J. Yang, P. X. Xiong, C. Zheng, H. Y. Qiu and M.D. Wei, *J. Mater. Chem. A*, 2014, **2**, 16640-16644; (c) J.

Yang, C. Zheng, P. X. Xiong, Y. F. Li and M. D. Wei, *J. Mater. Chem. A*, 2014, **2**, 19005-19010.
21 D. Y. Lee, D. V. Shinde, E. Kim, W. Lee, I. Oh, N. K. Shrestha, J. K. Lee, S. H. Han, *Microporous Mesoporous Mater.*, 2013, **171**, 53-57.
22 A. Morozan and F. jaouen, *Energy Environ. Sci.*, 2012, **5**, 9269-9290
23 A. Fateeva, P. Horcajada, T. Devic, C. Serre, J. Marrot, J. M. Grenèche, M. Morcrette, J. M. Tarascon, G. Maurin and G. Ferey, *Eur. J. Inorg. Chem.*, 2010, **24**, 3789-3794.
24 J. E. Halls, D. M. Jiang, A. D. Burrows,M. A. Kulandainathanb and F. Marken, *Electrochemistry*, 2013, **12**, 187-193.
25 (a) I. Jung, J. Choi and Y. Tak, *J. Mater. Chem.*, 2010, **20**, 6164-6169; (b) T.T. Liu, G. J. Shao, M. T. Ji and Z. P. Ma, *Ionics*, 2014, **20**, 145-149.
26 (a) Y. Munaiah, B. G. S. Raj, T. P. Kumar and P. Ragupathy, *J. Mater. Chem. A*, 2013, **1**, 4300-4306; (b) Z. Jiang, W. J. Lu, Z. P. Li, K. H. Ho, X. Li X. L. Jiao and R. D. Chen, *J. Mater. Chem. A*, 2014, **2**, 8603-8606.
27 H. H. Huo, Y. Q. Zhao and C. L. Xu, *J. Mater. Chem. A*, 2014, **2**, 15111-15117.